PRAMANA
— journal of
physics

Vol. 57, Nos 2 & 3
Aug. & Sept. 2001
pp. 611–622

Magnetic rotation and chiral symmetry breaking

ASHOK KUMAR JAIN and AMITA
Department of Physics, University of Roorkee, Roorkee 247 667, India

Abstract. The deformed mean field of nuclei exhibits various geometrical and dynamical symmetries which manifest themselves as various types of rotational and decay patterns. Most of the symmetry operations considered so far have been defined for a situation wherein the angular momentum coincides with one of the principal axes and the principal axis cranking may be invoked. New possibilities arise with the observation of rotational features in weakly deformed nuclei and now interpreted as magnetic rotational bands. More than 120 MR bands have now been identified by filtering the existing data. We present a brief overview of these bands. The total angular momentum vector in such bands is tilted away from the principal axes. Such a situation gives rise to several new possibilities including breaking of chiral symmetry as discussed recently by Frauendorf. We present the outcome of such symmetries and their possible experimental verification. Some possible examples of chiral bands are presented.

Keywords. Chiral symmetry; magentic rotation.

PACS Nos 21.60.-n; 21.10.-k

1. Introduction

Rotation is a universal phenomenon. The macroscopic world is replete with the examples of objects (planets, stars and galaxies) rotating independently and coherently at the same time. The microscopic world however places a severe restriction on rotational motion. A molecule or a nucleus must be anisotropic or, non-spherical in nature. While no such restriction exists for the celestial objects, it was Jacobi who concluded that 'ellipsoids with three unequal axes can very well be figures of equilibrium' [1]. Riemann later showed that ellipsoidal figures of equilibrium are possible under three circumstances: (a) the case of uniform rotation ($\vec{\omega}$ = constant) with no internal motions ($\vec{\zeta} = 0$, vorticity of internal motion), (b) the case when $\vec{\omega}$ and $\vec{\zeta}$ coincide with a principal axis of the ellipsoid, and (c) the case when the direction of $\vec{\omega}$ and $\vec{\zeta}$ lie in a principal plane of the ellipsoid. The case (b) corresponds to the principal axis cranking. In case (c), we see the appearance of a planar tilted axis cranking. We thus have the new possibility of triaxial shapes rotating about an axis other than one of the principal axes. The rotational motion is of course more complex in nuclei. Still we are able to see emergence of analogous situations and more.

The normal rotation in nuclei is associated with the presence of a significant electric quadrupole moment. As a result, one obtains enhanced electric quadrupole transitions connecting $\Delta I = 2$ levels in a rotational band. Regions of deformed nuclei where rotational motion is observed, are now well defined and generally lie between the magic numbers.

Spherical nuclei are few and remain confined to the proximity of magic numbers. It was therefore very surprising when regular rotational-like features were seen in nuclei lying close to the magic numbers [2,3]. The group of levels first seen in the Pb isotopes display enhanced magnetic dipole transitions connecting $\Delta I = 1$ level sequences. Observation of such rotational structures has created much excitement in nuclear physics akin to the one created after the discovery of the superdeformed bands. These bands have been variously termed as the 'magnetic dipole', 'magnetic rotational' or, 'shears' band.

2. Magnetic rotation bands and the shears mechanism

Amita *et al* [4] adopted the following criteria to characterize the MR bands:

- These are $\Delta I = 1$ sequences with strong M1 transitions.
- The B(M1) values are large (of the order of a few μ_N^2).
- Crossover E2 transitions are either absent or very weak.
- The deformation should be small, preferably $\beta_2 \leq 0.15$.
- The dynamical moment of inertia $\Im^{(2)}$ ranges from 10 to 25$\hbar^2$ MeV^{-1} which is smaller than the values in normal and superdeformed nuclei. Also, the ratio $\Im^{(2)}/B(\text{E2}) > 100$ MeV^{-1} eb^{-2} is much larger than the typical values in normal and superdeformed nuclei.

The collection of bands presented by Amita *et al* [4] presents more than 120 bands localized in four mass regions: $A = 80$ ($Z = 35$–37), 110 ($Z = 48$–51), 135 ($Z = 54$–64), and 195 ($Z = 80$–86). The lead region alone accounts for more than 42 bands. These mass regions coincide with those theoretically expected on the basis of the configurations which support the shears mechanism. This collection classifies the experimentally observed level structures according to their intrinsic configurations and other measured properties such as B(M1)/B(M2) values, lifetimes and other features. A number of high spin features such as signature splitting, signature inversion and backbending have also been observed.

As we go up in energy in a rotational band, the increase in angular momentum can come from a combination of two sources: collective and/or, single particle motion. However, magnetic rotational bands have been interpreted in a slightly different way. While the source of generating the angular momentum is single particle (few particles involved), its outcome is rotation-like. The shears mechanism suggested by Stefan Frauendorf [5] can be understood from the example of a MR band in ^{105}Sn. It may be noted that historically the first MR band was identified in Pb-mass region which have a slightly oblate shape. Since then, MR bands have been seen in nuclei which are slightly prolate also. For example, Sn isotopes possess a small prolate deformation.

The ^{105}Sn isotope has 50 protons (filling up the $Z = 50$ shell completely) and 55 neutrons. The last protons fill up the $g_{9/2}$ orbital (see figure 1). One of the $g_{9/2}$ pair of protons breaks up and gets excited to the $g_{7/2}$ orbital. The lowest lying and most suitable proton configuration turns out to be $\pi(g_{9/2}^{-1} \otimes g_{7/2})$.

The $g_{9/2}$ proton hole and the $g_{7/2}$ proton particle combination drives the nucleus towards slightly prolate shape. The neutrons above the $N = 50$ shell gap occupy the $g_{7/2}, d_{5/2}$ and $h_{11/2}$ orbitals. The possible configuration for the lowest MR band in ^{105}Sn may be

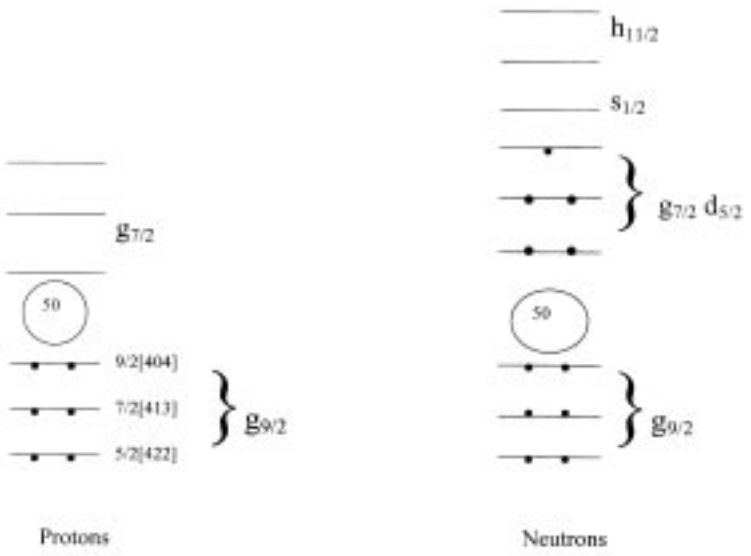

Figure 1. Ground state configuration of protons and neutrons in ^{105}Sn.

given by $\pi(g_{9/2}^{-1}g_{7/2}) \otimes \nu(h_{11/2}^2(d_{5/2}g_{7/2})^1)$. Near the bandhead, the proton hole gives us a dumbbell-like density distribution with its angular momentum pointing along the 3-axis whereas the neutron particle gives a torus-like density distribution with its angular momentum pointing along the 1-axis. The proton and the neutron angular momenta at this point are perpendicular to each other and the resultant angular momentum points between the two (tilted at an angle to the 1-axis). As we go up the band, the total angular momentum increases due to a gradual alignment of the proton and the neutron angular momenta into the direction of the total angular momentum. The process resembles that of a closing of a pair of shears and hence the name 'shears mechanism'.

In figure 2, we show the situation at two different rotational frequencies. At a lower rotational frequency, figure 2a, the proton and the neutron blades are nearly perpendicular to each other. The magnetic moment components of the neutron and the proton along the total angular momentum and perpendicular to it are also shown here. Since neutrons have a negative magnetic moment, it points opposite to the neutron angular momentum. The components of the magnetic moment along the total angular momentum tend to cancel each other whereas the components perpendicular to it add up. The perpendicular component $\mu_\perp$ thus gives rise to an anisotropy in the currents. It is this anisotropy that leads to magnetic rotation. We thus have a 'magnetic top' rather than an ordinary rotating top. At a higher rotational frequency, the proton and neutron blades come closer together and give rise to a resultant higher in angular momentum (see figure 2b).

The closing of the blades with increasing rotational frequency has an interesting consequence on the M1 transition probability. Since the B(M1) values are directly proportional to the square of the perpendicular component of the magnetic moment $\mu_\perp$, it decreases as the blades close because the $\mu_\perp$ decreases. This is one of the most remarkable characteristics of the MR bands and therefore an experimental indicator of the existence of shears mechanism. This prediction has recently been tested in lifetime measurements [6].

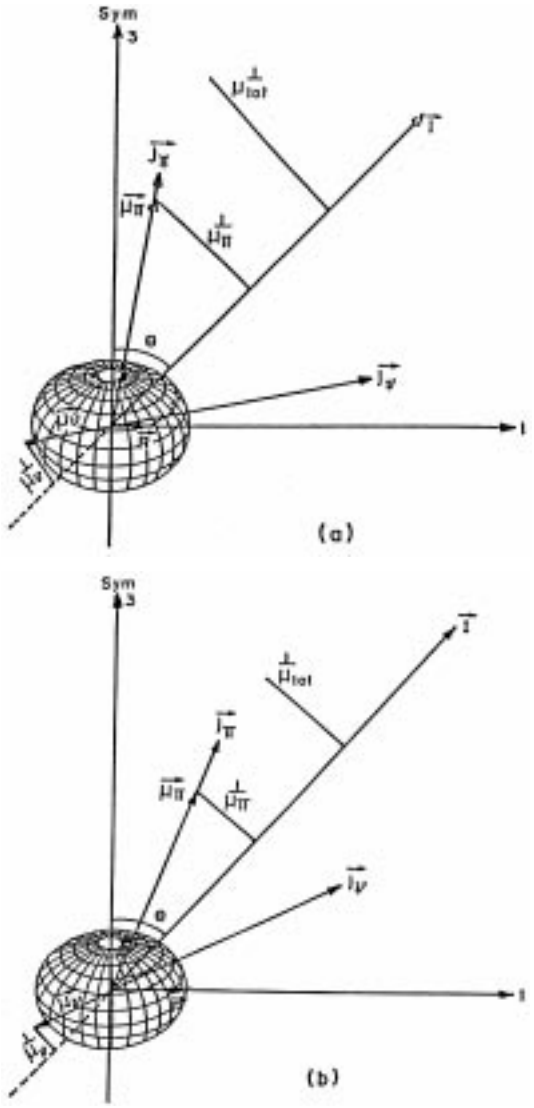

Figure 2. Schematic coupling scheme of shears mechanism for a small oblate deformation at (**a**) small rotational frequency, and (**b**) larger rotational frequency.

3. Tilted axis cranking

There are two important differences that arise between the familiar picture of principal axis cranking (PAC) and the tilted axis cranking (TAC) proposed for such kind of situations as depicted by the MR bands. Whereas normal deformed nuclei are mostly axially symmetric spheroids with $\gamma = 0$, the γ-deformation plays an important role in MR bands and the mean field can rotate about an axis other than the principal axis (Riemann ellipsoid).

The first fully self-consistent solutions of TAC were presented by Frauendorf [5]. The approximation provides solutions which were interpreted as $\Delta I = 1$ bands and are now widely used to describe the MR bands as well as high-K bands [7]. The mean field Routhian is fixed by two deformation parameters ϵ and γ and two polar angles θ and ϕ, which fix the orientation of $\vec{\omega}$ with respect to the principal axes. A general TAC Routhian may look like,

$$h'_{\rm TAC} = h_{\rm s.p.} - \Delta(P^+ + P) \\ -\lambda\hat{N} - \omega(j_1 \sin\theta\cos\phi + j_2 \sin\theta\sin\phi + j_3\cos\theta), \quad (1)$$

where $h_{\rm s.p.}$ is the single particle Hamiltonian of a deformed field (e.g. a deformed oscillator or, a deformed Woods–Saxon potential). The total angular momentum $\vec{J}$ is tilted with respect to the principal axis by two polar angles θ and ϕ. The Routhian also contains a pairing potential and a number conserving term. The choice $\phi = 0^\circ$ corresponds to a planar tilt i.e. the rotation is about an axis tilted in one of the principal planes. A non-zero value of ϕ leads to the more general situation of aplanar TAC.

3.1 *A schematic model*

In a simple toy model of planar TAC, we choose a particle in a high-j orbital

$$h' = h_{\rm def} - \omega[j_1 \sin\theta + j_3\cos\theta], \quad (2)$$

where

$$h_{\rm def} = \kappa\Big[\frac{3m^2}{j(j+1)} - 1\Big] \quad (3)$$

and $\kappa = 51.5A^{-1/3}\beta$. We have used $A = 110$, $\beta = 0.1$ and $j = 11/2$ for a schematic calculation of single particle routhians.

The results of our numerical calculations for $\theta = 90^\circ, 70^\circ, 45^\circ$, and 10° are shown in figure 3.

The value $\theta = 90^\circ$ corresponds to the principal axis cranking where rotation is about 1-axis. We can see that as the rotational frequency increases, the time-reversal degeneracy is lifted and the Nilsson states (at $\omega = 0$) split into two. This is due to the Coriolis force which breaks the time-reversal symmetry and acts strongly on the low-Ω states. As a result, the splitting is quite large for low-Ω states. The signature is still a good quantum number and we get $\Delta I = 2$ bands. For $\theta = 70^\circ$, the routhians show a most remarkable change. We note that all the states begin to split quite early and the splitting of higher lying states increases as θ increases. This may be understood in terms of an increasing Coriolis effect on higher Ω states as the projection on rotation axis decreases with increasing θ. It now becomes possible for both low-Ω and high-Ω states to align towards the rotation axis which is lying in the middle. It may be remarked that Ω is no longer a good quantum number but is still a good label to identify the states. This explains the tendency of particle as well as hole states, having their angular momenta perpendicular to each other, to align along a rotation axis lying in the middle. Presence of a triaxial shape where $\gamma \neq 0$ (Riemann ellipsoids) further appears to facilitate the rotation about a tilted axis.

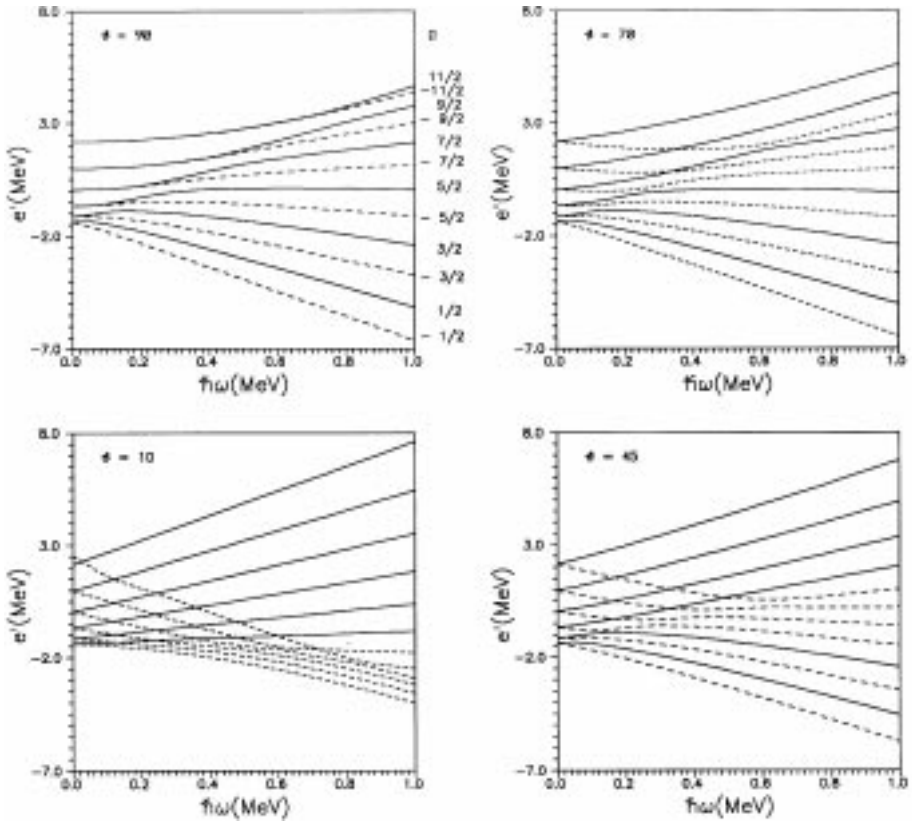

Figure 3. Single particle routhians using the schematic TAC model hamiltonian given in eq. (2) for $j = 11/2$ and the tilt angles $\theta = 90^\circ, 70^\circ, 45^\circ$ and 10°.

3.2 *Results from the general TAC routhian*

The features described above are also present in the results of general TAC routhian. As an example, we present the results for the case of ^{105}Sn, using the pairing plus quadrupole–quadrupole version of the TAC [8]. In figure 4, we show the results of single proton routhians for the $Z = 50$ magic number for $\theta = 70^\circ$.

If we focus our attention on the high-j $h_{11/2}$ orbital, its behaviour is found to be very similar to that shown in figure 3 for $\theta = 70^\circ$. The observed MR band in ^{105}Sn has a bandhead spin 29/2$^+$ which can be obtained by a multiparticle configuration [4]. As already discussed, the breaking of a $g_{9/2}$ pair gives the configuration $(g_{9/2}^{-1} g_{7/2})$ for protons. The neutrons involve coupling of $g_{7/2}d_{5/2}$ quasi-neutrons with $h_{11/2}$ quasi-neutrons. This combination gives the correct spin, parity and excitation for the band under consideration. The total energy was minimized in the laboratory frame and gave a deformation $\beta_2 = 0.137$ and $\gamma = 0$. The TAC results for this configuration along with the experimental routhian are shown in figure 5 in the form of I vs. $\hbar\omega$ plot.

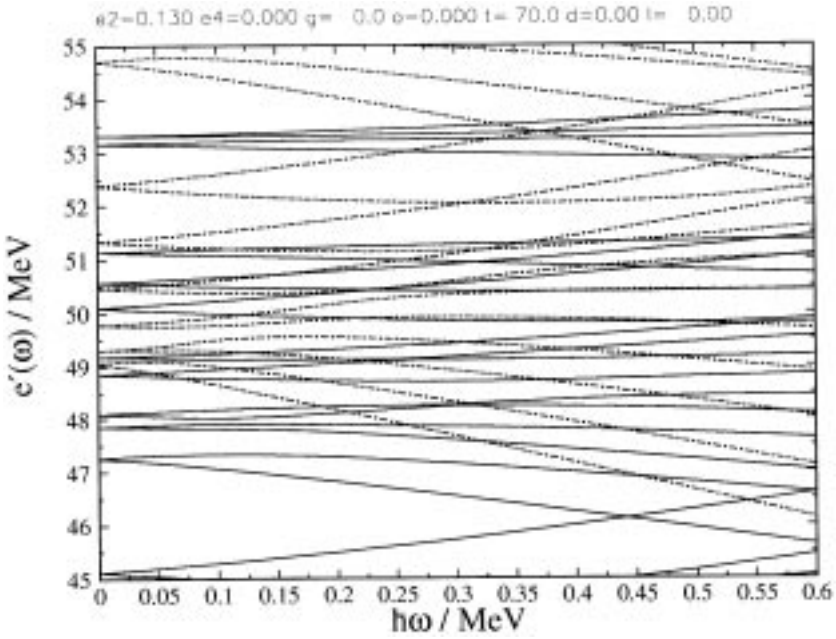

Figure 4. Single proton routhians for $Z = 50$ and $\theta = 70^{\circ}$ by using the general TAC hamiltonian. The six pair of dashed lines from the bottom correspond to $h_{11/2}$ orbital.

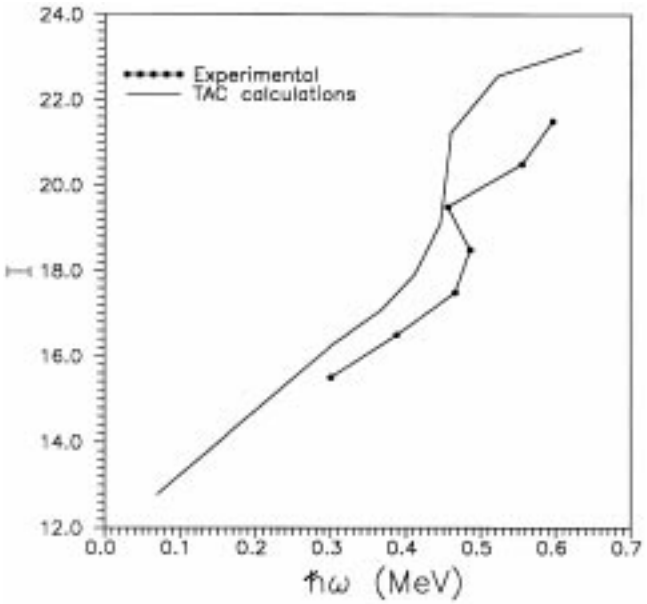

Figure 5. I vs. $\hbar\omega$ plot for the MR band in ^{105}Sn using the TAC model.

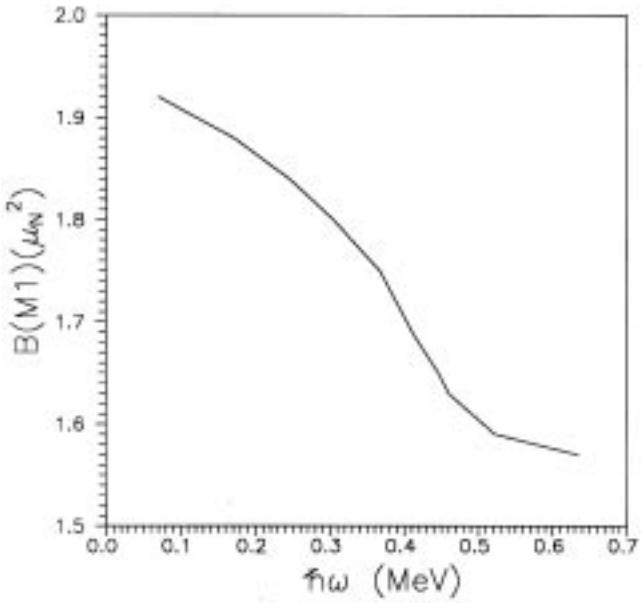

Figure 6. B(M1) vs. $\hbar\omega$ for the MR band in ^{105}Sn using the TAC model.

The experimental curve is reproduced quite well for a tilt angle $\theta = 70^\circ$. The B(M1) values can be calculated in the TAC model by using the expressions given in [9]. The result of our calculation is shown in figure 6. The B(M1) values decline sharply with increasing rotational frequency providing a strong support for the shears mechanism in this band.

4. Symmetries

Symmetries of the mean field play an important role in the classification of rotational spectra. Breaking of the isotropy of the mean field is a necessary condition for the appearance of rotational bands. Bohr and Mottelson [10] present a detailed discussion of the geometrical symmetries of the intrinsic wave function and their consequences for the rotational spectra. Their discussion, however, remains confined to rotation about a principal axis.

In our discussion, we denote the body-fixed axes (intrinsic frame) by 1, 2, 3 and the space fixed axes (laboratory frame) by x, y, z. The three basic symmetries that survive at high spin are [7],

- $\wp$, space inversion,
- $\Re_z(\pi)$, rotation about the z-axis by an angle of π,
- $T\Re_y(\pi)$, time reversal and rotation about the y-axis by an angle of π.

All the symmetry operations listed above are 2-fold and commute with each other. Breaking up of any of these will lead to a doubling in the number of energy levels. Fraunedorf lists 15 different combinations which break the three symmetries; this includes the

breaking of the reflection symmetry and the octupole degree of freedom. We shall, however, not consider the effect of breaking the reflection symmetry and the octupole degree of freedom. Rather, we confine ourselves to triaxial shapes where all the three planes (1–2, 2–3, 1–3) have a reflection symmetry (D_{2h} symmetry). The nucleus therefore has a triaxial shape with one long axis (*l*), one intermediate axis (*i*) and one short axis (*s*). In figure 7, these are labelled as 3, 2 and 1 respectively. The space fixed axes are labelled as x, y and z and rotation axis is always taken as the z-axis.

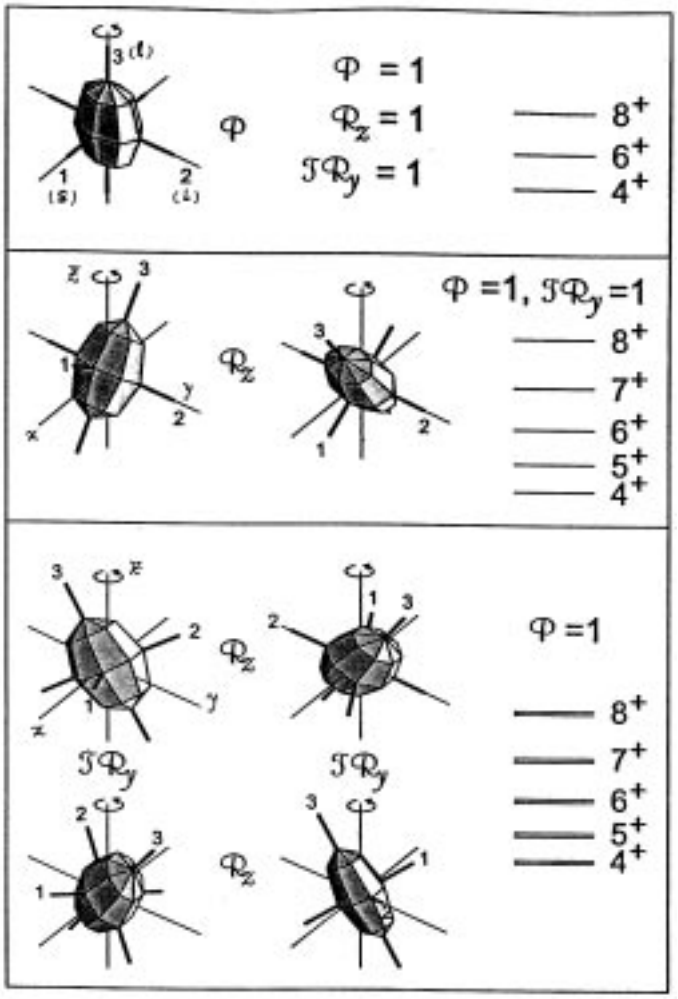

Figure 7. The symmteries of the mean field having D_{2h} symmetry. The rotation is considered about the space-fixed z-axis which coincides with the angular momentum $\vec{J}$. The top panel has all the three symmetries as noted in figure. $R_z(\pi)$ symmetry breaks down in the middle panel. The $TR_y(\pi)$ symmetry further breaks in the bottom panel giving rise to chiral symmetry breaking (from [12]).

4.1 *Signature quantum number*

Consider the case when the rotation axis coincides with one of the principal axes, say the long axis.

It is well-known that for spheroidal shapes where the γ-degree of freedom has been suppressed, only $K = 0$ bands having angular momentum $I = 0, 2, 4, \ldots$ are allowed for even–even nuclei. However, if $\gamma \neq 0$, it is possible to have $K = 2, 4, \ldots$, etc. and the band begins at $I = K$. A classification of states arises if the mean field configuration $|\rangle$ has $\Re_z(\pi)$ symmetry and $\Re_z(\pi)|\rangle = \mathrm{e}^{-i\alpha\pi}|\rangle$, where α is the signature quantum number. Invariance of h' with respect to it requires that the angular momentum I and α are related as

$$I = \alpha + \text{ even number.} \tag{4}$$

Thus the signature removes every other I from the rotational spectrum. The upper panel of figure 7 exhibits this situation for an even–even nucleus. Each quasi-particle configuration can be labelled by parity and signature quantum number (π, α).

4.2 *Ellipsoid with D_{2h} symmetry and a planar tilt*

The middle panel of figure 7 describes the situation when the axis of rotation is tilted from the principal axes and lies in one of the principal planes of the ellipsoid ($\theta \neq 0\,^\circ, 90^\circ; \phi = 0^\circ$).

We still have $\wp = 1$ but $\Re_z(\pi)$ symmetry is broken. As a consequence, signature is no longer a good quantum number and there is no restriction on I. We get a $\Delta I = 1$ rotational band instead of two $\Delta I = 2$ sequences. However, $T\Re_y(\pi)$ is still a good symmetry. A simple working model to verify these symmetries can be made by using a matchbox which has its three sides $a \neq b \neq c$. By sticking pins on all the six faces (body fixed axes), and one pin along the axis of rotation or J (space fixed z-axis), it becomes very easy to check and verify the various symmetry operations. It may be remembered that the time reversal operator T reverses the direction of rotation and $\Re_y(\pi)$ puts it back.

4.3 *Ellipsoid with D_{2h} symmetry and an aplanar tilt*

The bottom panel describes the situation of rotation about an aplanar tilted axis. An odd–odd triaxial nucleus provides an ideal example where such a situation may arise. If the odd proton configuration is such that the alignment is along the short axis, the valence neutron configuration is such that its alignment is along the long axis and the rotational contribution is along the intermediate axis (as the moment of inertia about this axis is maximum and the rotational energy is minimum) [11]. The three angular momenta are perpendicular to each other and the resultant angular momentum acquires an aplanar tilt. While parity remains unaffected, such an arrangement breaks the $T\Re_y(\pi)$ symmetry. The two situations shown in the upper part of this panel have a right handed sense of rotation with respect to the frame of reference (1,2,3). On the other hand, the two situations shown in the lower part have left-handed sense of rotation with respect to the (1,2,3) frame. The breaking of the

$T\Re_y(\pi)$ symmetry in systems with even number of fermions, doubles the number of levels and we should observe two pairs of identical $\Delta I = 1$ bands having the same parity. These are the chiral bands where the chiral symmetry has been broken. In real nuclei, however, the bands may have some mixing because of a tunelling between the right-handed and the left-handed states; it will show up as a splitting between the two bands. It may be noted that existence of triaxiality and an optimum quadrupole deformation play an important role in breaking the chiral symmetry.

Dimitrov *et al* [12] have recently presented the first results of an aplanar TAC calculation which supports the existence of chiral bands in ^{134}Pr. In figure 8, we present four such possible cases of chiral bands including ^{134}Pr. The case of ^{108}Sb is quite remarkable because the splitting of the levels is very small. The other two examples are of even–even nuclei and involve six-qp and four-qp configurations in ^{106}Sn and ^{136}Nd respectively. It may be noted that ^{106}Sn ($\beta = 0.11, \gamma = -13°$) is already considered to be a very good case of magnetic rotation and the proximity of the bands in energy may not be due to chirality. Recent claims have also been made of observing chiral pair of bands in ^{130}Cs, ^{132}La, ^{136}Pm and ^{118}I [13], and ^{136}Pm and ^{138}Eu [14]. Theoretical calculations are, therefore, required to verify the chirality in these bands.

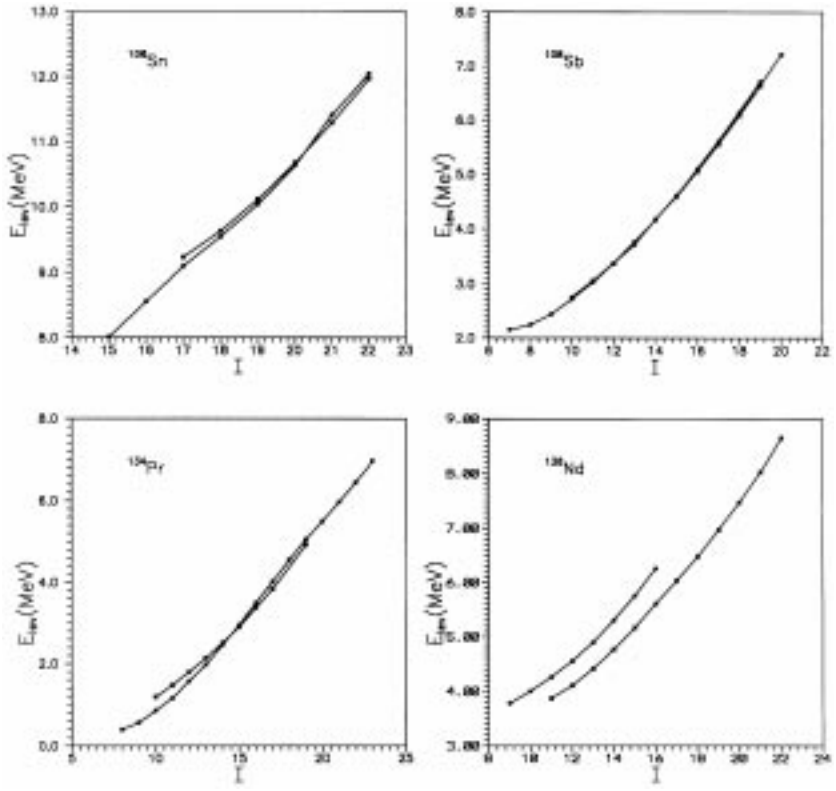

Figure 8. Possible examples of chiral pair of bands.

5. Conclusions

We have presented the phenomenon of magnetic rotation which allows rotational bands to be observed in near-spherical nuclei. Further, the shears mechanism responsible for the MR bands provides a new way of generating the angular momentum. Salient features of magnetic rotational bands have been summarized. The tilted axis cranking model incorporates the shears mechanism and has been very successful in explaining the salient features of these bands. A toy model explaining the effect of TAC on single particle orbitals was presented. The results of a general TAC calculation for ^{105}Sn were also presented. Finally, we have considered the effect of tilted axis cranking on the symmetries of the mean-field at high spin. It is pointed out that TAC may lead to a number of new situations where spontaneous breakdown of symmetry may occur and therefore a number of new types of characteristic rotational patterns may emerge. We have confined ourselves to the discussion of symmetry breaking in an ellipsoid having D_{2h} symmetry. The appearance of chiral rotational bands is pointed out and some possible examples of chiral bands are also presented.

Acknowledgement

Financial support from the Department of Science and Technology (Govt. of India) and Council of Scientific and Industrial Research (Govt. of India) is acknowledged.

References

[1] S Chandrashekhar, *Ellipsoidal figures of equilibrium* (Yale University Press, New Heaven, 1969)
[2] H Hubel *et al*, *Prog. Part. Nucl. Phys.* **28**, 427 (1992)
[3] R M Clark *et al*, *Phys. Lett.* **B275**, 247 (1992)
[4] Amita, A K Jain and B Singh, *At. Data Nucl. Data Tables* **74**, 283 (2000)
[5] S Frauendorf, *Nucl. Phys.* **A557**, 259c (1993)
[6] R M Clark *et al*, *Phys. Lett.* **B440**, 251 (1998)
[7] S Frauendorf, *Rev. Mod. Phys.* **73**, 463 (2002)
[8] Amita and A K Jain, *Nuclear structure and dynamics* edited by A K Jain and R K Bhowmik (Phoenix publishing, New Delhi, 2000) 60
[9] S Frauendorf and J Meng, *Nucl. Phys.* **A617**, 131 (1997)
[10] A Bohr and B R Mottelson, *Nuclear structure* (Benjamin, New York, 1975) vol. 2
[11] J Meyer-ter-Vehn, *Nucl. Phys.* **A249**, 111 (1975)
[12] V I Dimitrov, S Frauendorf and F Donau, *Phys. Rev. Lett.* **84**, 5732 (2000)
[13] K Starosta, T Koike, C J Chiara, D B Fossan and D R La Fosse, *Nucl. Phys.* **A682**, 375c (2001)
[14] C W Beausang *et al*, *Nucl. Phys.* **A682**, 394c (2001)